Chapter 2
Impact of Climate Change on the Availability of Virtual Water Estimated with the Help of Distributed Neurogenetic Models

Mrinmoy Majumder, Sabyasachi Pramanik, Rabindra Nath Barman, Pankaj Roy, and Asis Mazumdar

Abstract Impact of climate change on virtual water of a tropical multireservoir system was estimated with the help of models developed by neural network and genetic algorithm. Virtual water or embedded water or embodied water, or hidden water refers to the water used in the production of goods or services. For instance, it takes 1,300 m^3 of water on an average to produce 1 t of wheat. The precise volume can be more or less depending on climatic conditions and agricultural practice. The virtual water has major impacts on productive use of water and global trade policy especially in water-scarce regions.

M. Majumder (✉)
Senior Research Fellow, School of Water Resources Engineering, Jadavpur University, Kolkata-700032, West Bengal, India
and
Geo-information Scientist, Regional Center, National Afforestation and Eco-development Board, Jadavpur University, Kolkata-700032, West Bengal, India
e-mail: mrinmoy@majumder.info

S. Pramanik
Assistant Engineer, Durgapur Projects Limited, Bardhaman, West Bengal, India
and
Former PG Student, School of Water Resources Engineering, Jadavpur University, Kolkata-700032, West Bengal, India

R.N. Barman
Pertime Research Fellow, School of Water Resources Engineering, Jadavpur University, Kolkata-700032, West Bengal, India
and
Assistant Professor, Department of Production, National Institute of Technology, Agartala, Tripura, India

P. Roy
Lecturer, School of Water Resources Engineering, Jadavpur University, Kolkata-700032, West Bengal, India

A. Mazumdar
Coordinator, Regional Center, National Afforestation and Eco-development Board, Jadavpur University, Kolkata-700032, West Bengal, India
and
Director, School of Water Resources Engineering, Jadavpur University, Kolkata-700032, West Bengal, India

B.K. Jana and M. Majumder (eds.), *Impact of Climate Change on Natural Resource Management*, 19
DOI 10.1007/978-90-481-3581-3_2,

The impact of climate change on virtual water could open a path for the efficient use of virtual water in the face of climatic uncertainties, which may directly impact availability of raw water. The present study tried to estimate the future virtual water with the help of neurogenetic models, which estimates stream flow as function of various hydrological, meterological variables, and basin characteristics. The models prepared were distributed in nature and also consider temporal variability. In total, two models were prepared with rainfall, time of concentration, and catchment loss as input and stream flow as output. One model was prepared by classifying the dataset, based on the magnitude of the variable, and the other model was prepared with normal dataset. First, the better performing model was identified and then output from RCM-PRECIS model was applied to the chosen model to estimate the impact of climate change on stream flow. The estimation results were used to calculate the amount of virtual water, and the result was compared with the present-day virtual water to analyze the change in virtual water availability due to climate change. According to the results, model prepared with normal dataset was identified as a better model, and from the estimations it could be concluded that virtual water availability would increase in case of both A2 and B2 scenario of climate change where the change would be more pronounced in case of the latter.

Keywords Climate change • water availability • virtual water • neurogenetic models

2.1 Introduction

Global warming is defined as a natural or human-induced increase in the average global temperature of the atmosphere near the Earth's surface. The earth as a planet is a complex combination of many elements, which constitute the solid earth, atmosphere, biosphere, cryosphere, and the hydrosphere. These components interact with each other in a nonlinear manner involving the feedbacks of energy, mass, and momentum. The energy is derived from the sun in the form of short-wave solar radiation, which penetrates the Earth surface with little loss of energy in transit. In the process, the heated Earth emits thermal or long-wave radiation outward, which mostly gets absorbed by the atmospheric constituent. Water vapor and several other gases including carbon dioxide, methane, and CFCs warm the Earth's atmosphere because they absorb and remit radiations. They trap some of the heat energy radiations from the Earth's atmospheric system. The trapping or warming is somewhat analogous to a greenhouse, which also traps heat; thus, the process has been called the greenhouse effect. The excessive increase in the concentration of green house gases (GHGs) makes the atmosphere warmer, which in turn induce the climate to change.

2.1.1 Impact of Global Warming

The effect of global warming is now predominant in many parts of the world. Twelve warmest years have occurred in 1900s among which 10 have occurred between 1987

and 1998. The energy availability, which was increased due to increase in temperature, had created a ripple effect throughout the Earth system with local, regional, and global positive feedbacks feeding on each other to amplify and accelerate warming (Stewart et al. 2006). Abnormality in climatic pattern, induced by the accelerated warming, had started to effect catchment-specific hydrologic cycles. In the last 10 years, floods have caused more damage than in the previous 30 years. Higher temperatures lead to a higher rate of evaporation and very dry conditions in some areas of the world. Severe weather events are now more common. The number and strength of hurricanes, tornadoes, and other events had increased over the last 15–20 years. As per IPCC (2007), global climate change is expected to affect the performance of water resource systems according to current indicators and findings.

2.1.2 Climate Models

The uncertainty in the climatic pattern had made the estimation of future climate more complex. Global Climate Model (GCM) were widely used to estimate future climatic parameters, but the complexity of the present climatic pattern had forced many modifications. HadCM2 AOGCM model was developed by Met Office Hadley in 1994 and its successor, HadCM3 AOGCM (Atmosphere-Ocean General Circulation Models), was published in 1998. AOGCM coupled with an atmospheric chemistry model, which can predict the changes in the concentration of other atmospheric constituents in response to climate change and to the changing emissions of various gases was later built on 1999. In HadCM3, thermohaline circulation, ventilation, and vertical mixing of chemical constituents along with decadal variability in the ocean were included.

Local climate change is influenced greatly by local features such as mountains, which are not well represented in global models (GCMs) because of their coarse resolution, and models of higher resolution could not practically be used for global simulation for long periods of time due to spatial variance of the considered parameters. These problems were tried to be mitigated with the help of regional climate models (RCM). The RCM had higher resolution (typically 50 km) were constructed for limited areas and allowed to run for shorter periods (20 years or so). The Met Office Hadley Centre had run RCMs for three regions: Europe, the Indian subcontinent, and southern Africa and had developed an RCM to run on PCs for any region as part of a regional climate modeling system called "Providing REgional Climates for Impacts Studies (PRECIS)."

PRECIS is based on the Hadley Centre's regional climate modeling system. It has been ported to run on a PC (under Linux) with a simple user interface, so that experiments can easily be set up over any region. PRECIS was developed in order to help generate high-resolution climate change information for as many regions of the world as possible. The intention is to make PRECIS freely available to groups of developing countries in order that they may develop climate change scenarios at national centers of excellence, simultaneously building capacity and drawing on local climatological expertise. These scenarios can be used in impact, vulnerability, and adaptation studies, and to aid in the preparation of National Communications, as required under Articles 4.1 and 4.8 of the United Nations Framework Convention on Climate Change. A more detailed description of climate models was given in Chapter 23.

The estimations from these climatic models were applied to hydrologic models to estimate the future impacts of climate change on different hydrologic parameters as explained in the next section.

2.1.3 Coupled Climatic and Hydrologic Models

A dynamic downscaling method, referred as pseudowarming, was used by Fujihara et al. (2008) to connect the output of raw general circulation models (GCMs) into river basin hydrologic models, which was applied to explore the potential impact of climate change on hydrology and water resources of the Seyhan River Basin in Turkey. The results showed that the decreased precipitation as formulated by the climate model would result in a considerably decreased inflow and time of peak. Hotchkiss et al. (2000) predicted the changes in global river flow under the IPCC SRES A1B and A2 scenarios found from HadGEM1-TRIP model and concludes that there will be significant change in the seasonality of river flow, such as earlier peaks in spring runoff, large increases in monthly maximum flow, and decreases in monthly minimum flow. Climatologic data bases (SICLIM and CLICOM) built by the Servicio Meteorológico Nacional (SMN) of Mexico (Mendoza et al. 2008) were fed to a hydrologic model to predict the annual volume of superficial available water. A climate variability indicator (the El Niño-Southern Oscillation, ENSO) was applied by Muluye and Coulibaly (2007) to predict seasonal reservoir inflows. GCM, CGCM2, CSIROMk2, and HadCM3 was applied by Merritt et al. (2006) to estimate future water availability of Okanagan Basin in England. Each of the research work advocates decrease in quantity of water as the common effect of climate change.

2.1.4 Application of Computer Models in Hydrology

The complexity of interrelationship of hydrometeorological parameters enforced hydrologic engineers to employ computer models with conditional variability to estimate future pattern of important hydrological parameters such as reservoir inflow (El-Shafie et al. 2007); Long et al. 2007); Kim et al. 2007), reservoir operation (He et al. 2008), and reservoir optimization (Wei and Hsu 2007; Majumder et al. 2007; Eslami and Mohammadi 2002; Xu and Li 2001; Luo and Weiss 2002). Single-event models such as HECHMS, TR55, MODRAT, etc., were widely employed by many engineers all over the world. A detailed description about hydrologic models is given in Chapter 21.

2.1.4.1 Application of Artificial Neural Network in Hydrology

In recent years, artificial neural networks (ANNs) had been successfully applied in forecasting of time series problems. As ANNs offer a relatively quick and flexible means of modeling, the application of ANN modeling was widely reported in various hydrological

literatures (Zhang and Stanley 1999; Neelakantan and Pundarikanthan 2000; Ray and Klindworth 2000) such as for rainfall–runoff modeling (Hsu et al. 1995; Fernando and Jayawardena 1998; Tokar and Johnson 1999; Elshorbagy et al. 2000; Liong et al. 2001), for stream flow prediction (Clair and Ehrman 1998; Imrie et al. 2000), for reservoir inflow forecasting (Jain et al. 1999; Coulibaly et al. 2000), and for water quality parameters (Maier and Dandy 1999). All the papers reported high degree of satisfaction and advocates for neural network as a promising alternative for improved hydrologic predictions. For a more detail description about neural network and genetic algorithm refer Chapter 22.

2.1.4.2 Virtual Water and Its Impacts

Water-scarce countries like Israel discourage the export of oranges (relatively heavy water guzzlers) precisely to prevent large quantities of water being exported to different parts of the world. In recent years, the concept of virtual water trade has gained weight both in the scientific and in the political debate. The notion of the concept is ambiguous. It changes between an analytical, descriptive concept and a political induced strategy. As an analytical concept, virtual water trade represents an instrument, which allows the identification and assessment of policy options not only in the scientific, but also in the political discourse. The data that underlie the concept of virtual water can readily be used to construct water satellite accounts, and brought into economic models of international trade such as the GTAP Computable General Equilibrium Model (Berrittella 2007). Such a model can be used to study the economic implications of changes in water supply or water policy, as well as the water resource implications of economic development and trade liberalization. In sum, virtual water trade allows a new, amplified perspective on water problems.

In the framework of recent developments from a supply-oriented to a demand-oriented management of water resources it opens up new fields of governance and facilitates a differentiation and balancing of different perspectives, basic conditions, and interests. Analytically, the concept enables to distinguish between global, regional, and local levels, and their linkages. This means that water resource problems have to be solved in problemsheds (Allan 1998) if they cannot be successfully addressed in the local or regional watershed. Virtual water trade can thus overcome the hydro-centricity of a narrow watershed view.

2.1.4.3 Limitations of Virtual Water Concept

The virtual water concept proposed by Allan has some serious shortcomings, which could impact the conclusions found from trend analysis of virtual water. The next section highlights a few of the major limitations:

1. The virtual water concept assumes all sources of water, whether in the form of rainfall or provided through an irrigation system, is of equal value.
2. Implicitly assumes that water that would be released by reducing a high water use activity would necessarily be available for use in a less water-intensive activity.
3. Fails as an indicator of environmental harm.

2.1.5 Objective and Scope

The model in the present study was prepared to estimate stream flow with the help of ANN and input variables like rainfall, time of concentration, and loss coefficient. The output from climatic model, RCM-PRECIS, was then applied to the model to estimate the impact of climate change on stream flow. The soil condition, land use and bed slope, travel length of water, and distance from the catchment centroid was calculated with the help of remote-sensed images of the study area and GIS. The land use and soil conditions were used to calculate loss coefficient of the catchment. The bed slope, length of water travel, and length from the centroid to the river was applied to calculate time of concentration with the help of Bend County method. Groundwater balance was included with hydrological variables along with water level. In climatological variables rainfall of each of the gauge station and distributed rainfall from TYNDAL dataset for ungauged stations were used in the development of the model. In case of reservoirs, reservoir storage along with reservoir level was included in the hydrological variables. The estimated stream flow from the model was used to calculate virtual water, that is, the amount of water used in the industries within the catchments. Basin discharge of a station is added to the same of next station after removing channel loss to get the discharge of the next station. The channel loss was calculated by dividing area of sediments from total area of the channel between two gauge stations and subtracting the result from 1. In case of reservoirs, monthly values of storage coefficient were calculated and multiplied with the basin discharge of the same place to get the actual discharge of the location. The storage coefficient was calculated with the help of storage-discharge routing or modified pulse routing method. The result is normalized to estimate the storage coefficient. In summary, it may be said that the main objective of the study was to estimate the availability of virtual water in face of climatic uncertainties but scopes of the study included estimation of stream flow, loss coefficient, and channel loss with the help of GIS along with estimation of storage coefficient with the help of Modified Pulse Routing.

2.1.6 Study Area

The impact of climatic uncertainties on availability of virtual water was shown on two major river networks of East India, Damodar and Rupnarayan. Both the river networks have many industries within their catchment. A detailed description of the two river networks and its industrial status are given in Chapter 25.

2.2 Methodology

The present study developed two models to predict stream flow of the gauged and ungauged catchments of rivers Damodar and Rupnarayan for 2010–2100, according to A2 and B2 scenario of climate change (Chapter 23). The predicted stream flow

was later applied to the equation of water availability and from the water availability, amount of available virtual water was determined.

Neural network was used to prepare the two models, whereas genetic algorithm was applied to find the most suitable network architecture. The model was trained with three types of training algorithms to identify or learn the encoded pattern within considered input and output variables. The better trained model was identified with the help of three performance validation criteria. The selected model was calibrated by comparing with the observed stream flow data and validated with the output from HECHMS, TR55, and MODRAT model.

2.2.1 Neurogenetic Spatially Distributed Rainfall–Runoff Model (NSRRM)

2.2.1.1 Model Variables of NSRRM

The NSRRM was developed to consider the influence of metereologic and hydrologic variables along with basin characteristics upon basin runoff. Peak average monthly rainfall of 32 years (1970–2002) and 12 months, monthly time of concentration, and monthly variation of loss coefficient of the basins at 42 sampling points were used to predict peak average monthly basin runoff at the same 42 selected sampling points. In Neurogenetic models, inputs are multiplied with a weightage and then summed to estimate the output after going through an activation function. If differences exist between estimated and desired output the operation is repeated again with updated weightage value until and unless the estimated and desired output becomes equal or a desired root mean square error (RMSE) calculated with the help of the two values is achieved. That is why, in the present model, peak rainfall, time of concentration, and loss coefficient were multiplied and used as input. The same value was subtracted from peak discharge and the difference was used as output variable of the present model so that during the iteration procedure, less computational energy and time was required to learn the problem.

Determination of Peak Average Monthly Rainfall and Runoff

The peak average monthly rainfall or runoff was calculated with the help of daily rainfall and runoff dataset for 32 years (1970–2002). As there were 42 sampling points, and if datasets for each of the sampling points were considered, the size of dataset becomes too large (483,840) for the computational facilities available for the present study. Hence, monthly average values were calculated for each month of each year, from which peak average monthly values were taken as the dataset of present study. In this procedure, size of the dataset becomes 505, which was possible for the computational facilities available for the present study and also reduces the amount of time required to develop the models.

Determination of Basin Loss Coefficient

SPOT imageries collected from different years and months of the sampling points and within 15/15 km grid around the channel was processed with a commercial software. The images were classified according to the DN values of different geographical features so that pixel with same DN values gets categorized into a single class. The DN values of different geographical features were identified and used to categorize the images into classes of different geographical features. Common geographical features of the study area includes forest, cropped and noncropped agricultural fields, ponds, industrial areas, mines, roads and pavements, etc. The area of each geographical class was calculated and divided from the total area. A weighted average of the output of each geographical class was determined where a feature with high runoff retention capacity like forest, pond, etc., was given lower weightage and feature with low runoff receptivity was given higher value of weightage. The result is subtracted from 1 to get the loss coefficient. Imageries of different months and years were used to determine loss coefficient of different months and years. The values were then averaged to get the average monthly loss coefficient of sampling points.

Determination of Channel Loss Coefficient

The channel loss was calculated with the help of the concept utilized to determine loss coefficient. Instead of geographical features of a basin, same of the channels were considered. Channels may have sand dunes and/or agricultural fields. Sand dunes are known to have higher infiltration capacity than agricultural fields. The same weighted average method was used to calculate loss coefficient of channels. Imageries of different months and years were collected to determine channel loss of different months and years.

Determination of Loss Coefficient

The channel loss coefficient along with basin loss coefficient was averaged to estimate the loss coefficient at the sampling points.

Calculation of Time of Concentration

Time of concentration was calculated with the help of Fort Bend County (Wanielista et al. 1997) method. The value of the inputs like length of longest flow path, average slope along longest flow path, average basin slope, and percentage impervious area were calculated with the help of GIS. Fort Bend County method was expressed by the following equation:

$$t_c = 48.64 \times \left(\frac{L}{S^{0.5}} \right)^{0.57} \times \mathrm{Log} \left(\frac{S_0}{S_0^{0.11} \times 10^I} \right) \tag{1}$$

where t_c is the time of concentration (h), L is the length of longest flow path (mi), S is the average slope along longest flow path (ft/mi), S_0 is the average basin slope (ft/mi), and I is the percent impervious area.

Fort Bend County method can be used for calculation of time of concentration only if the area of the catchment is within 0.13–400 mi², the longest flow path lies between 0.5 and 55 mi, slope along the longest flow path will lie in between 2 and 33 ft/mi, and the average basin slope will lie within 3–80 ft/mi. As all the subwatersheds considered in the present study satisfy the above conditions, Fort Bend County method was utilized for estimation of time of concentration (Wanielista et al., 1997).

2.2.1.2 Model Development

Three 2.1 input–1 output variable neurogenetic models were developed and trained with QP, CGD, and BBP algorithm, which were respectively named as NSRRMQP, NSRRMCGD, and NSRRMBBP.

Table 2.1 showed the input and output variables of NSRRM hydrologic models and Fig. 2.1. depicts the overview of model algorithm.

2.2.2 Categorized Neurogenetic Spatially Distributed Rainfall–Runoff Model (CNSRRM)

The CNSRRM model was developed similar to NSRRM model except the datasets used for training the neural models were categorized into different groups. Neurogenetic models were found as a better learner of a problem when grouped data were used for training the models. Thus, the dataset was grouped and used to develop another kind of neurogenetic model.

2.2.2.1 Model Variable

Input variables for CNSRRM model were selected as grouped dataset of peak average monthly rainfall of 12 months and 32 years, monthly time of concentration,

Table 2.1 Table showing input and output variables used for the NSRRM model

Input	Abbreviation
Output	Abbreviation
Product of peak average monthly rainfall (P), time of concentration (t_c), and loss coefficient (L_c)	$p\{P, t_c, L_c\}$
Difference between peak average monthly basin runoff (Q) and product of average monthly rainfall (P), time of concentration (t_c), and loss coefficient (L_c)	$F[Q - \{P, t_c, L_c\}]$

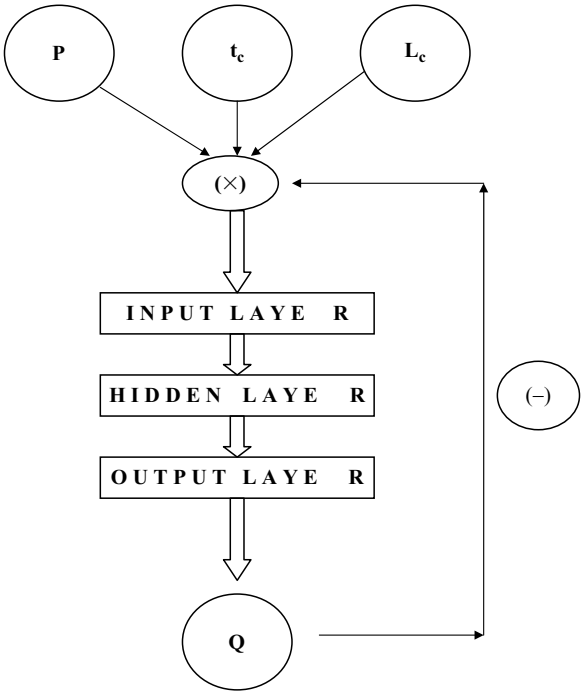

Fig. 2.1 Chart showing algorithms adopted to develop the NSRRM models

and monthly variation of loss coefficient at 42 sampling points. The output variable was selected as peak average monthly basin runoff. The dataset of the output variable was not categorized.

For the CNSRRM model, each variable was encoded into six classes in the following way:

1. The variable dataset was ranked in a descending order according to magnitude.
2. If the rank of a data was less than 5, then the data would cluster into HP class.
3. If the rank of a data was less than 25 and greater than 5, then the data would cluster into P class.
4. If the rank of a data was less than 50 and greater than 25, then the data would cluster into MP class.
5. If the rank of a data was less than 250 and greater than 50, then the data would cluster into MT class.
6. If the rank of a data was less than 500 and greater than 250, then the data would cluster into T class.
7. Remaining dataset was clustered into HT class.

The class/group notation HP, P, and MP separates the peak values from smaller values of the variable, which were again separately denoted by MT, T, and HT.

Table 2.2 shows the input and output variables of CNSRRM Hydrologic models and Fig. 2.2. depicts the overview of model algorithm

Table 2.2 Table showing input and output variables used for the CNSRRM model

Input	Abbreviation
Output	Abbreviation
Peak average monthly rainfall (P), time of concentration (t_c), and loss coefficient (L_c). (Dataset of all the variables were grouped into six classes according to their magnitude.)	P, t_c , L_c
Peak average monthly basin runoff (Q)	Q

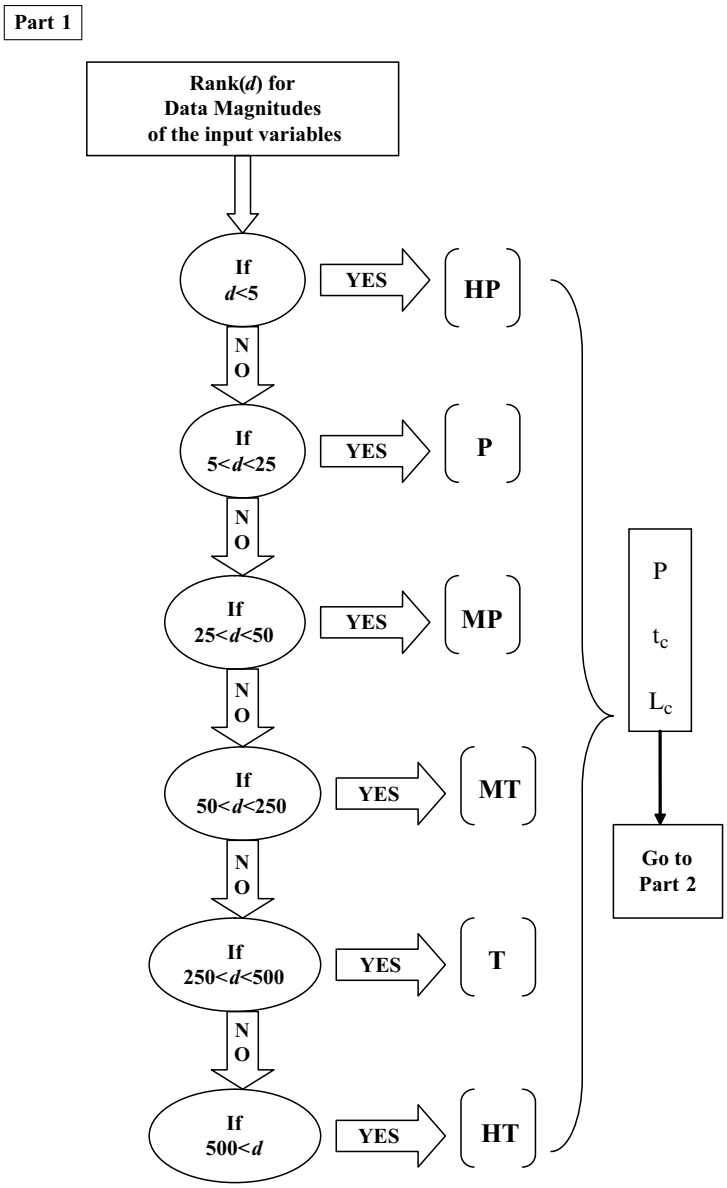

Fig. 2.2 *Part 1*: flowchart showing the conditions used for categorizing the dataset. *Part 2*: flowchart showing the architecture and dataflow of CNSRRM models

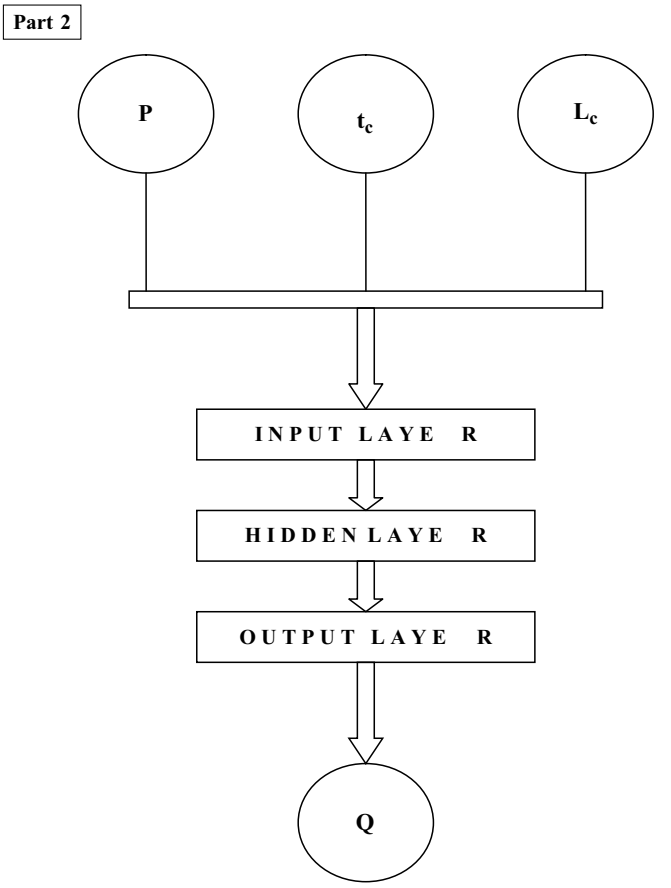

Fig. 2.2 (continued)

2.2.3 Model Validation and Uncertainty Analysis

The discharge from the sampling points was also estimated with the help of HECHMS, TR55, and MODRAT hydrologic model. The output from the three considered conceptual models along with neurogenetic models and observed discharge data were compared to calculate the RMSE (2.2), correlation coefficient (r) (2.3), coefficient of efficiency (E) (2.4), and first-order uncertainty analysis (U) (2.5) of the models. The values would help in selection of the better model among the six models considered in the present study.

$$\text{RMSE} = \sqrt{\sum_{n=1}^{n} \frac{(T_p - O_p)^2}{n}} \tag{2}$$

$$\text{Correlation coefficient} = \sqrt{\frac{\sum (T_p - T_m)(O_p - O_m)}{\sum_1^n (T_p - T_m)^2 \sum_1^n (O_p - O_m)^2}} \tag{3}$$

$$\text{Coefficient of efficiency} = 1 - \frac{\sum_{n=1}^{n} (T_p - O_p)^2}{\sum_{n=1}^{n} (T_p - T_m)^2} \tag{4}$$

$$\text{First - order uncertainty}(U) = \left(\frac{Stdev(O_p - O_m)}{n} \right) \tag{5}$$

where T_p is the target data value for the pth pattern; O_p is the estimated data value for the pth pattern, T_m and O_m are the mean of target and estimated datasets, respectively, and n is the total number of patterns. T_n is the target value of the nth pattern and T_m is the mean value of the targeted dataset.

Correlation coefficient could also be taken as a measure of model reliability whereas coefficient of efficiency was also used as a measure of model sensitivity (Das 1991) toward observed dataset. Hence, both of these validation criteria also help to determine model reliability and sensitivity where high values would represent greater level of reliability and sensitivity of the model.

2.3 Result and Discussion

According to the comparison results given in Table 2.3, RMSE of CNSRRMBBP was found to be 3.00, which was less than any other models. The RMSE of NSRRMQP (3.42), NSRRMBBP (3.44), and NSRRMCGD (4.15) models were found to have the nearest value to RMSE of CNSRRMBBP. But the model reliability or correlation coefficient (0.64) of CNSRRMBBP was found to better than only CNSRRMCGD (0.61). All the other four models had better correlation coefficient than the latter, like, NSRRMQP, NSRRMCGD, and NSRRMBBP had correlation coefficient equal to 0.98, 0.97, and 0.98, respectively. The efficiency of CNSRRMBBP was found to be 0.82, which was less than the other five models considered for the present study where NSRRMQP had better efficiency (0.99) than any other models. NSRRMQP model was found to have only 8.5% uncertainty, whereas the same for CNSRRMBBP was found to be equal to 8.82%. As NSRRM had higher efficiency, second highest correlation coefficient and minimum uncertainty than the considered models of the present study, NSRRMQP was selected as the better model among the neurogenetic models developed for the present study.

If conceptual hydrologic models, like HECHMS, TR55, and MODRAT, were compared with the selected neurogenetic model, NSRRMQP was found to have

Table 2.3 Table showing the comparison of performance validation criteria and model parameters of the neurogenetic models

	NSRRMQP	NSRRMCGD	NSRRMBBP	CNSRRMBBP	CNSRRMQP	CNSRRMCGD
Model variables						
Input	$p\{P, L_c, T_c\}$	$p\{P, L_c, T_c\}$	$p\{P, L_c, T_c\}$	P, L_c, T_c	P, L_c, T_c	P, L_c, T_c
Ouput	$F[Q - \{P, L_c, T_c\}]$	$F[Q - \{P, L_c, T_c\}]$	$F[Q - \{P, L_c, T_c\}]$	Q	Q	Q
Model parameters						
Network topology						
Network type	Feed forward	Feed forward	Feed forward	Feed forward	Feed forward	Feed forward
Network structure	1,8,1	1,17,1	1,15,1	3,2,2,1	2,1,1	2,1,1
Network weight	16	34	30	12	3	3
Training dataset	80	80	80	80	80	80
Testing dataset	10	10	10	10	10	10
Validation dataset	10	10	10	10	10	10
GA parameters						
Population	100	100	100	50	50	50
Generation	150	150	150	100	100	100
Penalty	6	6	6	6	6	6
Crossover rate	0.8	0.8	0.8	0.8	0.8	0.8
Mutation rate	0.2	0.2	0.2	0.2	0.2	0.2
Stop training condition						
MSE	0.05	0.05	0.05	0.05	0.05	0.05
Iteration	200	200	200	200	200	200
Generalization loss	5	5	5	5	5	5
Training algorithm parameters						

Algorithm name	QP	CGD	BBP	BBP	QP	CGD
Activation function	Sigmoid	Sigmoid	Sigmoid	Tanh	Tanh	Tanh
Learning rule	Supervised	Supervised	Supervised	Supervised	Supervised	Supervised
Learning rate	0.8	NR	0.8	0.8	0.8	NR
Momentum	NR	NR	0.8	NR	NR	NR
Propagation coefficient	1.75	NR	NR	1.75	1.75	NR
Training and testing results						
RMSE (training)	5.78	9	8.15	5.78	6.56	6.78
RMSE (testing)	10.51	13.5	16.3	6.05	15.66	12.76
Training stop reason	Generalization loss	Generalization loss	Generalization loss	Generalization loss	Generalization loss	Generalization loss
Model estimation results						
RMSE	3.42	4.11	3.44	3.00	4.15	5.78
Relationship	0.98	0.97	0.98	0.64	0.74	0.61
Efficiency	0.99	0.97	0.98	0.82	0.97	0.98
Uncertainties (%)	8.5	9.79	8.77	8.82	8.89	8.98

Table 2.4 Table showing comparison of performance validation criteria of neurogenetic model with conceptual hydrologic models

Model name	RMSE	r	E	U (%)
NSRRMQP	3.42	0.98	0.99	12
HECHMS	5.45	0.67	0.78	15
TR55	6.78	0.65	0.68	20
MODRAT	10.12	0.71	0.58	45

better RMSE than HECHMS (5.45), TR55 (6.78), and MODRAT (10.12) (Table 2.4) hydrologic models. The efficiency of the neurogenetic model (0.99) was also found to be higher than the any of the considered conceptual models, HECHMS (0.78), TR55 (0.68), and MODRAT (0.58). The coefficient of relationship or reliability (0.98) of NSRRMQP was also found to be higher among the four considered models. The uncertainty analysis of all the four models revealed that NSRRMQP had the minimum uncertainty (12%) than the conceptual models where HECHMS, TR55, and MODRAT had an uncertainty of 15%, 20%, and 45%, respectively.

As NSRRMQP has higher r and E and lower RMSE and U than the three considered hydrologic models. NSRRMQP was selected as the model for the estimation of future basin runoff according to the A2 and B2 baseline climate change scenarios, which were collected from generation of weather scenarios by PRECIS climatic model.

Two types of neural models were prepared. Length of the furthest path from where droplets of water may reach length from the centroid of the catchment and slope were used to calculate time of concentration with the help of Bend County method. The loss coefficient, that is, the variable, which represents the loss of incoming water was also estimated with the help of remote sensing and GIS. The estimated rainfall, calculated time of concentration, and loss coefficient were used as input variables to build the neurogenetic models, which would give stream flow as output.

Virtual water was calculated from the data of industrial demand of the two river basins. The amount of water supplied to the industries as raw water for production of their products is actually the amount of virtual water present in the catchment.

The steel industries were found to be the highest consumer of such water in case of both the river basin according to the data collected from Damodar Valley Corporation followed by chemical and coal industries. Although, coal industries are found only in Damodar catchments. The paper industries developed around Rupnarayan catchment is the third biggest consumer of raw water. The thermal power stations also used water for generation of steam but major part of the water consumed is returned to the river.

Figure 2.3 shows the present variation of virtual water within the selected sampling regions. Figures 2.4–2.9 show the variation of virtual water along the selected sampling regions within the two river basins according to the estimation of NSRRMQP model. Figures 2.10–2.13 and Table 2.5 depict district-wise, state-wise, and basin-wise distribution of virtual water.

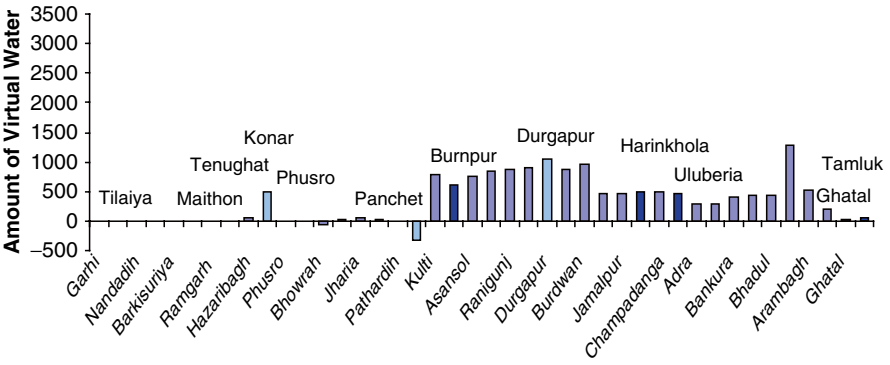

Fig. 2.3 Figure showing observed average available virtual water in different sampling regions considered in the present study (Note: columns with sky blue color represent virtual water of river junctions and columns with blue color represent virtual water at the reservoirs or barrages.)

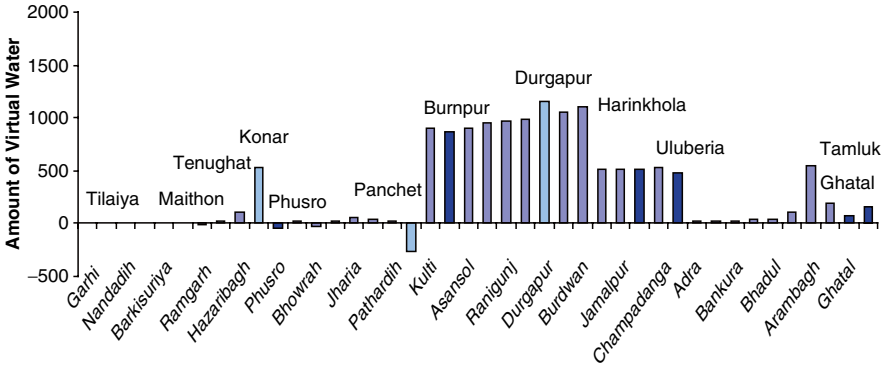

Fig. 2.4 Figure showing estimated available virtual water in different sampling regions considered in the present study from 2010 to 2040 in case of A2 scenario of climate change (Note: columns with sky blue color represent virtual water of river junctions and columns with blue color represent virtual water at the reservoirs or barrages.)

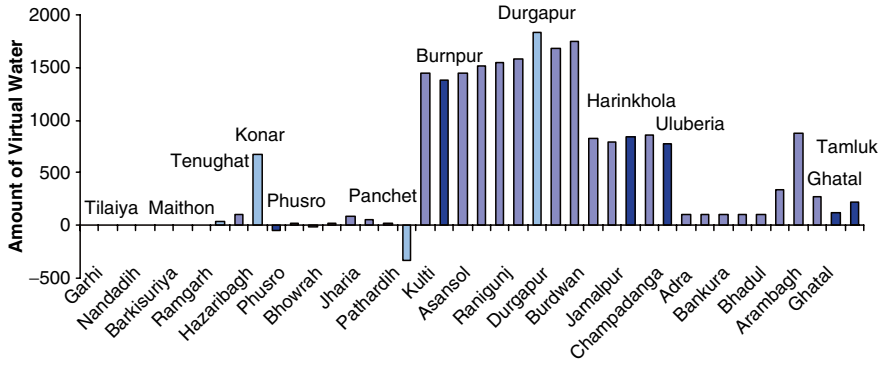

Fig. 2.5 Figure showing estimated available virtual water in different sampling regions considered in the present study from 2041 to 2070 in case of A2 scenario of climate change (Note: columns with sky blue color represent virtual water of river junctions and columns with blue color represent virtual water at the reservoirs or barrages.)

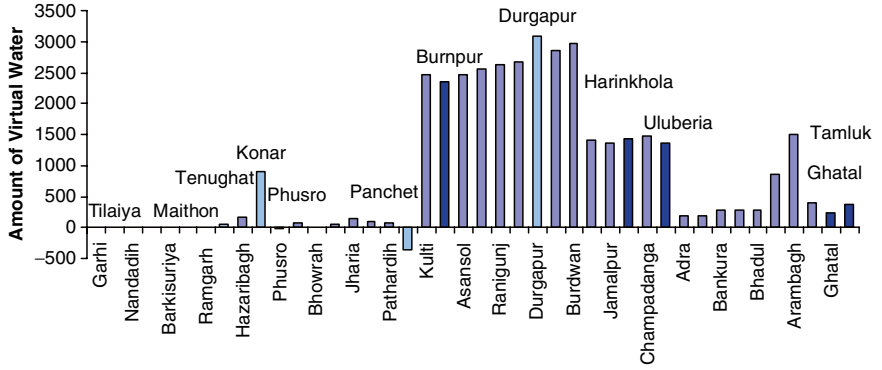

Fig. 2.6 Figure showing estimated available virtual water in different sampling regions considered in the present study from 2071 to 2100 in case of A2 scenario of climate change (Note: columns with sky blue color represent virtual water of river junctions and columns with blue color represent virtual water at the reservoirs or barrages.)

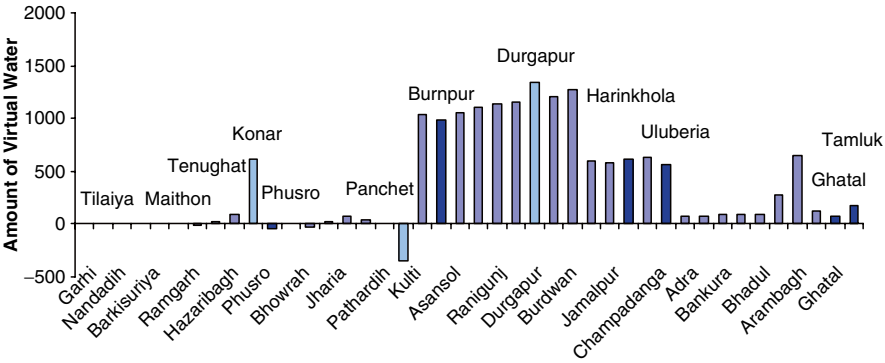

Fig. 2.7 Figure showing estimated available virtual water in different sampling regions considered in the present study from 2010 to 2040 in case of B2 scenario of climate change (Note: columns with sky blue color represent virtual water of river junctions and columns with blue color represent virtual water at the reservoirs or barrages.)

According to Table 2.5, Rupnarayan River Network and the state of Jharkhand would have more available virtual water in B2 scenario of climate change than in A2 scenario of climate change for 2010–2070 but from 2071 to 2100, the trend reverses where A2 scenario would have more available virtual water than B2 scenario. Similar but opposite trend was observed in Damodar River Network and state of West Bengal.

According to observed data of virtual water, West Bengal and Rupnarayan River Networks have more available virtual water than Jharkhand and Damodar River Networks. In the future, West Bengal would have more available virtual water than Jharkhand but when the two river networks were compared the trend would reverse in the future.

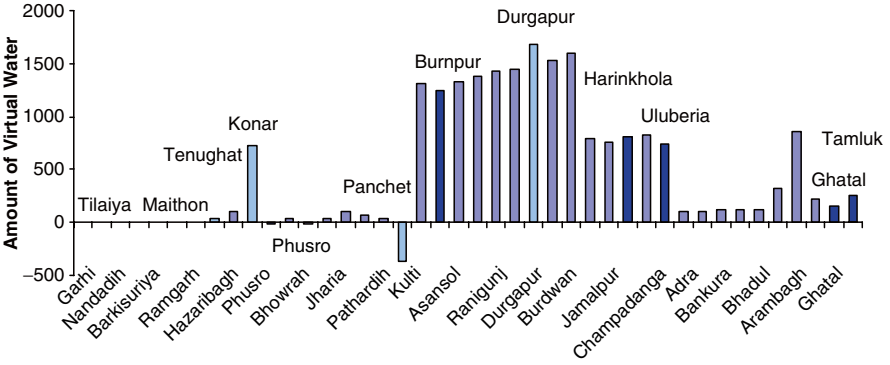

Fig. 2.8 Figure showing estimated available virtual water in different sampling regions considered in the present study from 2041 to 2070 in case of B2 scenario of climate change (Note: columns with sky blue color represent virtual water of river junctions and columns with blue color represent virtual water at the reservoirs or barrages.)

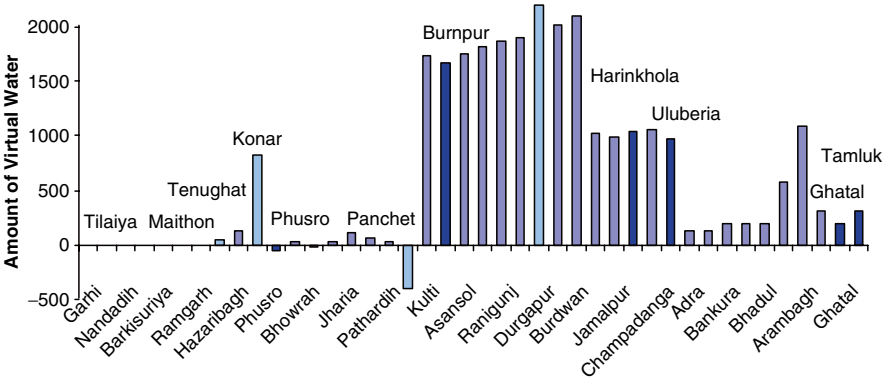

Fig. 2.9 Figure showing estimated available virtual water in different sampling regions considered in the present study from 2071 to 2100 in case of B2 scenario of climate change (Note: columns with sky blue color represent virtual water of river junctions and columns with blue color represent virtual water at the reservoirs or barrages.)

According to observed data of virtual water, Dhanbad, a district of Jharkhand, has a shortage and thus minimum amount of available virtual water and Hooghly, a district of West Bengal, has the maximum amount of available virtual water. The trend remains in the future from 2010 to 2100 for both the scenario of climate change except for 2071–2100 in A2 scenario of climate change when Jamtara becomes the district with minimum amount of available virtual water.

From Fig. 2.3, which represents the variation of virtual water within the sampling regions, it could be concluded that sampling regions of downstream than the same of upstream of both the river networks have more availability of virtual water. The trend remains that way from 2010 to 2100 though the magnitude of virtual water gets increased.

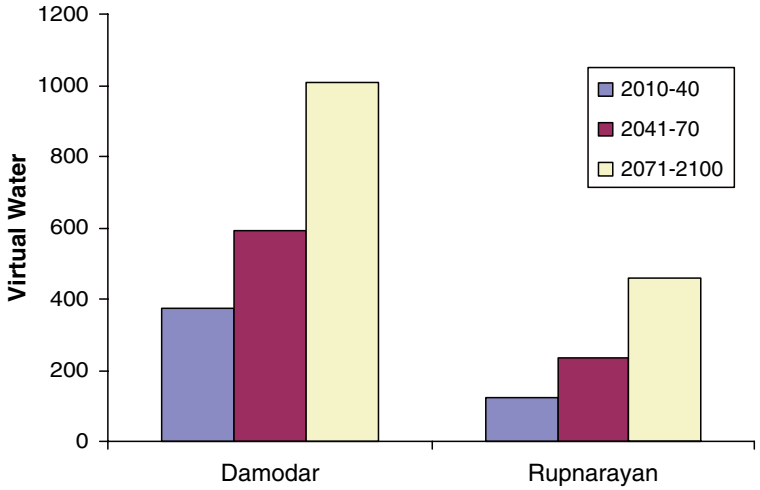

Fig. 2.10 Figure showing comparison of availability of virtual water in between Damodar and Rupnarayan Basins in case of A2 scenario of climate change

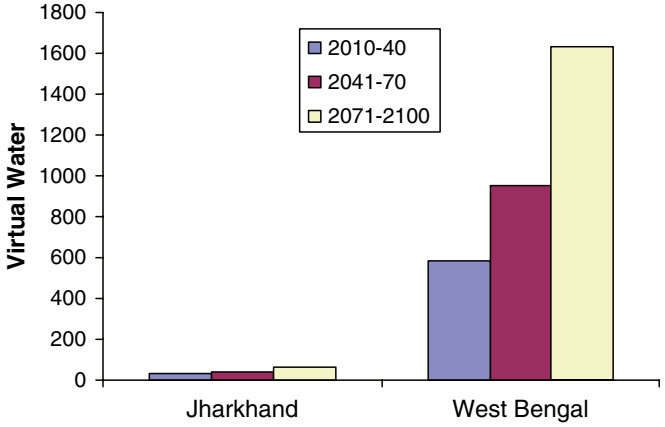

Fig. 2.11 Figure showing comparison of availability of virtual water within Jharkhand and West Bengal in case of A2 scenario of climate change

The above estimation of future availability of virtual water could be explained by the fact that virtual water availability is directly proportional to growth in industry. As industries are the only recipient of virtual water, if there is an increase in industrial consumer, the amount of virtual water will also increase. If the estimations of virtual water showed an increase in magnitude it could be concluded that there is a growth in industrial development and vice versa.

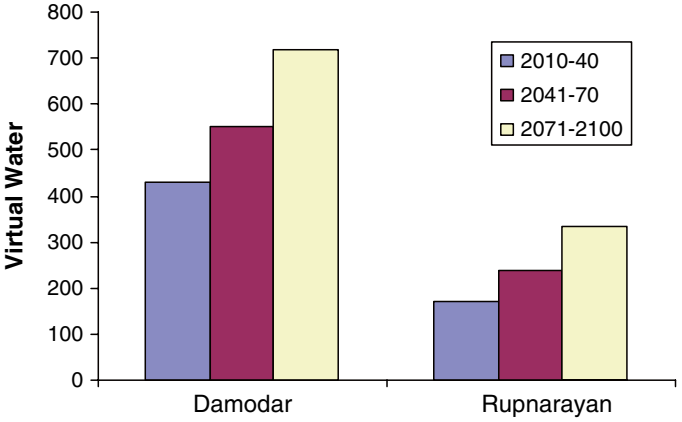

Fig. 2.12 Figure showing comparison of availability of virtual water in between Damodar and Rupnarayan Basins in case of B2 scenario of climate change

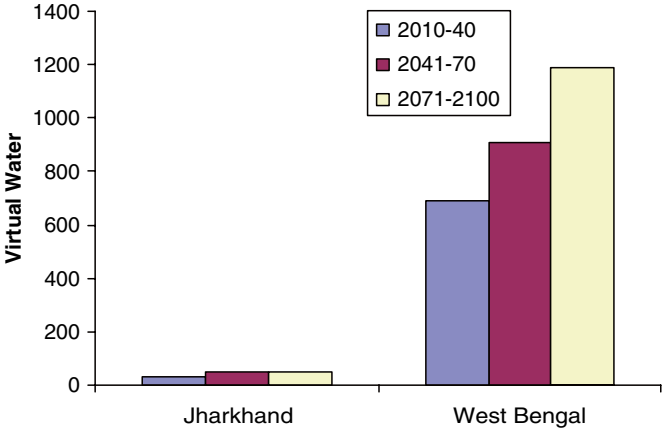

Fig. 2.13 Figure showing comparison of availability of virtual water within Jharkhand and West Bengal in case of B2 scenario of climate change

The districts of Burdwan and Hooghly of West Bengal and Hazaribagh districts of Jharkhand have a high concentration of industries like coal mines, steel, and paper, though industries, which consume maximum amount of water, as for example, steel, have a greater concentration in the former districts than the later. That is why, availability of virtual water is more in the districts of West Bengal (1,524.42 cm^3 in Hooghly) than in the district of Jharkhand (132.36 cm^3 in Hazaribagh).

Table 2.5 Table showing variation of virtual water within districts, states, and river basins due to A2 and B2 scenario of climate change

	A2 scenario			B2 scenario			Observed
Districts	2010–2040	2041–2070	2071–2100	2010–2040	2041–2070	2071–2100	1970–2002
State	2010–2040	2041–2070	2071–2100	2010–2040	2041–2070	2071–2100	1970–2002
Giridih	2.08	3.19	5.15	2.37	2.70	3.20	1.26
Jamtara	−0.79	−1.15	−0.92	−1.27	−1.08	−1.15	−0.51
Bokaro	1.10	1.73	2.78	1.18	1.51	1.73	0.35
Ranchi	11.80	14.60	25.60	12.04	22.00	17.78	4.47
Hazaribagh	196.71	245.76	344.30	218.79	272.23	299.37	132.36
Dhanbad	−18.70	−19.40	14.28	−35.41	−11.12	−22.86	−30.95
Burdwan	997.93	1,590.99	2,701.08	1,154.38	1,455.08	1,914.98	595.21
Hooghly	2,300.18	3,671.02	6,222.82	2,644.62	3,498.74	4,525.34	1,524.42
Howrah	487.23	781.95	1,359.69	571.73	747.64	973.00	327.69
Purulia	31.11	95.81	188.47	72.88	104.15	130.43	193.90
Bankura	46.70	150.96	374.22	121.78	155.34	259.23	392.67
West Midnapur	77.51	122.97	239.74	80.91	154.38	196.90	27.12
East Midnapur	151.89	229.47	365.49	174.93	261.17	310.75	44.43
Jharkhand	32.03	40.79	65.20	32.95	47.71	49.68	17.83
West Bengal	584.65	949.03	1,635.93	688.75	910.93	1,187.23	443.63
Basins	2010–2040	2041–2070	2071–2100	2010–2040	2041–2070	2071–2100	1970–2002
Damodar	373.02	591.11	1,010.30	429.36	552.56	716.54	223.91
Rupnarayan	124.20	235.62	457.03	172.15	237.19	333.67	273.04

2.4 Conclusion

The present study tried to estimate the impact of climate change on availability of virtual water of two subtropical river basins. The model estimation was carried out by the development of two types of neurogenetic models where input was treated as function of rainfall, time of concentration, and basin loss, and output was considered as difference between stream flow and product value of rainfall, time of concentration, and basin loss. The climate change impacts were analyzed with the help of rainfall data collected from A2 and B2 scenario of climate change generated by the PRECIS model and loss coefficient and time of concentration of the future were interpreted from IPCC fourth assessment report (2001). The predictions from the model, which were future stream flow, were used to calculate future availability of virtual water. According to the results, availability of virtual water would get increased in A2 scenario than in B2 scenario of climate change within the basins considered in the study. West Bengal would have more virtual water than Jharkhand, which actually follows the present trend of virtual water availability. The magnitude of virtual water showed increasing trend in both the scenario of climate change where the change is more pronounced in B2 than in A2 scenarios. As A2 baseline scenario was considered to be more economical than B2 and B2 scenario was considered to be more environmental than A2, the model results showed that becoming environmentally stable would actually be beneficial for virtual water, which also shows the industrial growth of a region. Hence, from the predictions, it could also be concluded that the future availability of water could mitigate the growing demand of water from the industries as model predictions of the sampling regions do not show a shortage of virtual water in any scenarios of climate change. As the models were developed with the help of neurogenetic algorithm, the model estimations were entirely based on the empirical relationship between the input and output variables. The models were also not flexible as it could only be used for the present two basins as neural models were data sensitive and would predict erroneously if data of one basin is applied to the other. Even with the above limitations, the selected model, NSRRMQP, had showed a relatively better accuracy of estimations (96.58%) than any other considered conceptual hydrologic models.

References

Allan JA (1998) Moving water to satisfy uneven global needs: 'trading' water as an alternative to engineering it, ICID Journal, 47(2):1–8. ISSN 0971-7412, September 1998

Berrittella M, Hoekstra AY, Rehdanz K, Roson R, Tol RSJ (2007) The economic impact of restricted water supply: A computable general equilibrium analysis, Water Research, 42: 1799–1813

Clair TA, Ehrman JM (1998) Using neural networks to assess the influence of changing seasonal climates in modifying discharge, dissolved organic carbon, and nitrogen export in eastern Canadian rivers. Water Resour Res 34(3):447–455

Coulibaly P, Anctil F, Bobee B (2000) Daily reservoir inflow forecasting using artificial neural networks with stopped training approach. J Hydrol 230(3–4):244–257
Das NG (1991) Statistical methods in commerce. Accountance and economics, M. Das & Co., Kolkata. Part – pp. 1.25–50
El-Shafie A, Taha MR, Noureldin AA (2007) Neuro-fuzzy model for inflow forecasting of the Nile River at Aswan high dam. Water Resource Manage 21(3):533–556
Elshorbagy A, Simonovic SP, Panu US (2000) Performance evaluation of artificial neural networks for runoff prediction. J Hydrol Eng 5(4):424–427
Eslami HR, Mohammadi K (2002) Application of ANN for reservoir inflow forecasting using snowmelt equivalent in the Karaj River watershed. Lowland Technol Int 4(2):17–26
Fernando DA, Jayawardena AW (1998) Runoff forecasting using RBF networks with OLS algorithm. J Hydrol Eng 3(3):203–209
Fujihara Y, Tanaka K, Watanabe T, Nagano T, Kojiri T (2008) Assessing the impacts of climate change on the water resources of the Seyhan river basin in Turkey. J Hydrol 353(1–2):33–48
He W, Chen J, Dai H (2008) Application of decision support system to the Three Gorges Reservoir operation. J Hydroelectric Eng 27(2):11–16
Hotchkiss RH, Jorgensen SF, Stone MC, Fontaine TA (2000) Regulated river modeling for climate change impact assessment: the Missouri River. J Amer Water Resource Assoc 36(2):375–386
Hsu K, Gupta HV, Sorooshian S (1995) Artifical neural network modeling of the rainfall-runoff process. Water Resour Res 31(10):2517–2530
Imrie CE, Durucan S, Korre A (2000) River flow prediction using neural networks: generalization beyond the calibration range. J Hydrol 233(3–4):138–154
IPCC (2007) Climate change 2007: the physical sciences basis, retrieved on http://ipcc-wg1.ucar.edu/wg1/wg1-report.html. on 30th April, 2009
Jain SK, Das A, Srivastava DK (1999) Application of ANN for reservoir inflow prediction and operation. J Water Resource Plan Manage 125(5):263–271
Kisi O (2004) Multilayer perceptrons with Levenberg–Marquardt training algorithm for suspended sediment concentration prediction and estimation. Hydrol Sci J 49(6):1025–1040
Kim Y-O, Eum H-I, Lee E-G, Ko IH (2007) Optimizing operational policies of a Korean multireservoir system using sampling stochastic dynamic programming with ensemble streamflow prediction. J Water Resource Plan Manage 133(1):4–14
Liong SY, Khu ST, Chan WT (2001) Derivation of Pareto front with genetic algorithm and neural network. J Hydrol Eng 6(1):52–61
Long ZQ, Zhang XH, Lin X-D, Chen ZJ (2007) Model for calculating benefit of forecasting intermediate inflow from downstream of reservoirs in water resources dispatch. J Hydraulic Eng 38(3):371–377
Luo W, Weiss E (2002) Evaluation of standard error of forecast of runoff volume using linear regression models. Can J Civil Eng 29(5):635–640
Majumder M, Roy P, Mazumdar A (2007) Optimization of the water use in the river Damodar in West Bengal in India: an integrated multi-reservoir system with the help of artificial neural network. J Eng Comput Architect 1(2) Online Journal: Article No. 1398
Maier HR, Dandy GC (1999) Empirical comparison of various methods for training feed-forward neural networks for salinity forecasting. Water Resour Res 35(8):2591–2596
Merritt WS, Alila Y, Barton M, Taylor B, Cohen S (2006) Hydrologic response to scenarios of climate change in sub watersheds of the Okanagan basin. Br J Hydrol 326:79–108
Mendoza VM, Villanueva EE, Garduño R, Nava Y, Santisteban G, Mendoza AS, Oda B, Adem J (2008) Thermo-hydrological modelling of the climate change effect on water availability in two hydrologic regions of Mexico. Royal Meteorological Society, Reading
Muluye GY, Coulibaly P (2007) Seasonal reservoir inflow forecasting with low-frequency climatic indices: a comparison of data-driven methods. Hydrol Sci J 52(3):508–522
Neelakantan TR, Pundarikanthan NV (2000) Neural network based simulation-optimization model for reservoir operation. J Water Resource Plan Manage 126(2):57–64
Ray C, Klindworth KK (2000) Neural networks for agrichemical vulnerability assessment of rural private wells. J Hydrol Eng 5(2):162–171

Stewart P, Le CF, Vemuri SR (2006) (Anticipated) Climate change impacts on Australia, Int J Ecol Dev 4:W06

Tokar AS, Johnson PA (1999) Rainfall-runoff modeling using artificial neural networks. J Hydrol Eng 4(3):232–239

US Army Corps of Engineers, Hydrologic Engineering Center (HEC). Hydrologic modeling system, HECHMS: technical reference manual. CPD-74B. US Army Corps of Engineers, Hydrologic Engineering Center, Davis, CA, http://www.hec.usace.army.mil/software/hec-hms/documentation/hms_technical.pdf, 2000

Wang QJ (1991) The genetic algorithm and its application to calibrating conceptual rainfall-runoff models. Water Resour Res 27(9):2467–2471

Wardlaw R, Sharif M (1999) Evaluation of genetic algorithms for optimal reservoir system operation. J Water Resour Plan Manage 125(1):25–33

Wang AP, Liao HY, Kou CH, Huang CY (2006) Artificial neural networks on reservoir inflows forecasting during typhoon season – a case in Taiwan. WSEAS Trans Math 5(4):416–422

Wei CC, Hsu NS (2007) Development of a real-time optimization model for flood control of a multipurpose reservoir. J Chinese Institute Civil Hydraulic Eng 19(3):355–365

Xu ZX, Li JY (2001) Short-term inflow forecasting using an artificial neural network model. Hydrological Processes, 16(12):2423–2439

Yitian L, Gu RR (2003) Modeling flow and sediment transport in a river system using an artificial neural network. J Environ Manage 31(1):122–134

Wanielista M, Kersten R, Eaglin R (1997) Hydrology: water quantity and quality control, 2nd edn. Wiley, New York

Zhang Q, Stanley SJ (1999) Real-time treatment process control with artificial neural networks. J Environ Eng 125(2):153–160